land

MDPI

Article

Emission Inventory of Soil Fugitive Dust Sources with High Spatiotemporal Resolution: A Case Study of Daxing District, Beijing, China

Qianxi Liu [1,2], Yalan Liu [1,2,*], Shufu Liu [1,*], Jinghai Zhao [3], Bin Zhao [3], Feng Zhou [3], Dan Zhu [3], Dacheng Wang [1,*], Linjun Yu [1,2], Ling Yi [1,2] and Gang Chen [1,2]

[1] Aerospace Information Research Institute, Chinese Academy of Sciences, Beijing 100101, China; liuqianxi22@mails.ucas.ac.cn (Q.L.); yulj201831@aircas.ac.cn (L.Y.)
[2] University of Chinese Academy of Sciences, Beijing 100049, China
[3] Daxing District Ecological Environment Bureau of Beijing Municipality, Beijing 102699, China
* Correspondence: liuyl@aircas.ac.cn (Y.L.); liusf@aircas.ac.cn (S.L.); wangdc@aircas.ac.cn (D.W.)

Abstract: Soil fugitive dust (SFD) is a significant contributor to environmental particulate matter (PM), which not only pollutes and affects air quality but also poses risks to human health. The emission inventory can provide a basis for the effective prevention and control of SFD pollution. However, current emission inventories with low resolution and frequency make it difficult to assess dust emissions accurately. Obtaining monthly high-resolution bare soil information is one of the solutions for compiling SFD emission inventories. Taking Daxing District, Beijing, as a case study, this study first extracted bare soil for each month of 2020, 2021, and 2022, respectively, using high-spatial-resolution remote sensing satellite data, and then constructed a 10 m-size emission grid and monthly SFD emission inventories based on the wind erosion equation by inputting vegetation cover factor, meteorological data, and soil erosion index. The total emissions of TSP, PM_{10}, and $PM_{2.5}$ in Daxing District from 2020 to 2022 were 3996.54 tons, 359.26 tons, and 25.25 tons, respectively. Temporally, the SFD emissions showed a decreasing trend over the years and were mainly concentrated in the winter and spring seasons. Spatially, the SFD emissions were predominantly concentrated in the southern and northern areas. And the emissions of PM_{10} exhibit a significantly stronger correlation with wind speed and the extent of bare soil area.

Keywords: soil fugitive dust; bare soil; wind erosion equation; emission inventory; remote sensing; high spatiotemporal resolution; air quality

Citation: Liu, Q.; Liu, Y.; Liu, S.; Zhao, J.; Zhao, B.; Zhou, F.; Zhu, D.; Wang, D.; Yu, L.; Yi, L.; et al. Emission Inventory of Soil Fugitive Dust Sources with High Spatiotemporal Resolution: A Case Study of Daxing District, Beijing, China. *Land* **2024**, *13*, 1991. https://doi.org/10.3390/land13121991

Academic Editor: Amrakh I. Mamedov

Received: 18 September 2024
Revised: 14 November 2024
Accepted: 20 November 2024
Published: 22 November 2024

1. Introduction

Bare soil areas are highly susceptible to soil erosion and serve as primary sources of pollution in urban microenvironments. PM generated from wind erosion poses a direct threat to environmental quality and public health [1–5]. SFD refers to PM originating directly from bare soil such as farmland, bare hillsides, mudflats, dry river valleys, undeveloped or non-vegetated land, etc., which form dust under the influence of natural forces or human activities (https://www.mee.gov.cn/gkml/hbb/bgth/201407/W020140708387894970380.pdf, accessed on 10 November 2024). It is considered a significant source of PM in northern China [6,7]. Unlike road and construction dust, the emission sources of soil dust are harder to pinpoint due to the effect of plant phenology and human activities (planting, harvesting), making it more difficult to identify the distribution of bare land [8]. Furthermore, research indicates that the contribution of soil dust sources to local emission inventories varies significantly across different regions, with discrepancies reaching up to four orders of magnitude [9–13]. The lack of appropriate inventory compilation methods may be a significant reason for the substantial discrepancies observed in these studies.

In fact, as early as the 1960s, the first-generation wind erosion equation (WEQ) developed by the United States Department of Agriculture had already been used to study dust emissions from bare land [14,15]. With a deeper understanding of wind erosion mechanisms, increasingly advanced models have been developed, such as the Revised Wind Erosion Equation (RWEQ) [16], the Wind Erosion Prediction System (WEPS) [17], and the Wind Erosion Model Simulation System (IWEMS) [18,19]. Although WEQ is less accurate than the newer models, its simplicity and strong operability make it easier to be promoted and applied [20]. WEQ was a recommended algorithm in its "Technical Guidelines for the Compilation of Emission Inventories for Dust Sources (Trial Version)" published in 2014 (https://www.mee.gov.cn/gkml/hbb/bgth/201407/W020140708387894970380.pdf, accessed on 10 November 2024). There are many application cases of WEQ in China [21–25], but there are some deficiencies. When using WEQ to estimate dust emissions, most studies adopted annual parameters (especially the area of soil dust sources); thereby, the seasonal variations in bare soil area were ignored [21–23]. The research by Liu [8] shows that the difference in bare soil area in the same region across different seasons can be up to seven times. On the other hand, the spatial resolution of the WEQ parameters obtained in research is relatively low, and the accuracy of the vegetation cover factor used in the calculations is insufficient [19,23]. These limitations result in inadequate spatiotemporal resolution of the WEQ, making it difficult to accurately estimate PM emissions in localized areas. Therefore, to develop high-spatiotemporal-resolution SFD emission inventories using WEQ, it is necessary to employ the appropriate methods to obtain parameters with higher spatiotemporal resolution.

Currently, some researchers employ satellite remote sensing (RS) to obtain high-spatial-resolution parameters and use geographic information systems (GISs) to process and analyze the data [26–28]. The use of RS and GISs has improved the efficiency of inventory compilation to a certain extent [20]. In order to accurately estimate the emissions of PM in localized areas and to develop high-spatiotemporal-resolution SFD emission inventories, this study has employed RS-GIS technology to obtain high-precision parameters, such as the area of bare soil dust sources and vegetation cover factors. Additionally, a 10 m × 10 m emission grid has been established to analyze the spatial distribution of bare soil dust emissions. It is anticipated that the results of this study will provide a scientific basis for air pollution control.

2. Materials and Methods

2.1. Study Area and Data Sources

Our study area is Daxing District, Beijing, which is located in the southern suburbs of Beijing. Geographically, it ranges from 39°26′ to 39°50′ north latitude and from 116°13′ to 116°43′ east longitude, with a total area of 1036.33 km^2. The soil in Daxing District is soft and conducive to cultivation. The region experiences a warm temperate, semi-humid continental monsoon climate with clearly defined seasonal variations. In spring, frequent winds and fluctuating temperatures prevail; in summer, high temperatures and ample rainfall dominate; in autumn, clear skies and minimal precipitation characterize the weather; and in winter, cold, dry conditions are accompanied by frequent winds and occasional snowfall [29]. As shown in Figure 1, the entire area of Daxing District is characterized by flat terrain with an elevation difference not exceeding 100 m. The meteorological stations within the district have good environmental representativeness, making them reliable for representing the climatic conditions (temperature, wind speed, precipitation) of the entire district [30]. The meteorological station in Daxing District is located in Jiugong Town, Daxing District, Beijing, with the station number 54511 (longitude: 116°28′, latitude: 39°48′). The built-up areas of Daxing District, including urban and industrial zones and roads, are concentrated in the northern and central parts (https://esa-worldcover.org/en, accessed on 10 November 2024), while Daxing International Airport is located in the southern part. Significant areas of bare soil around the airport and construction sites pose notable environmental challenges.

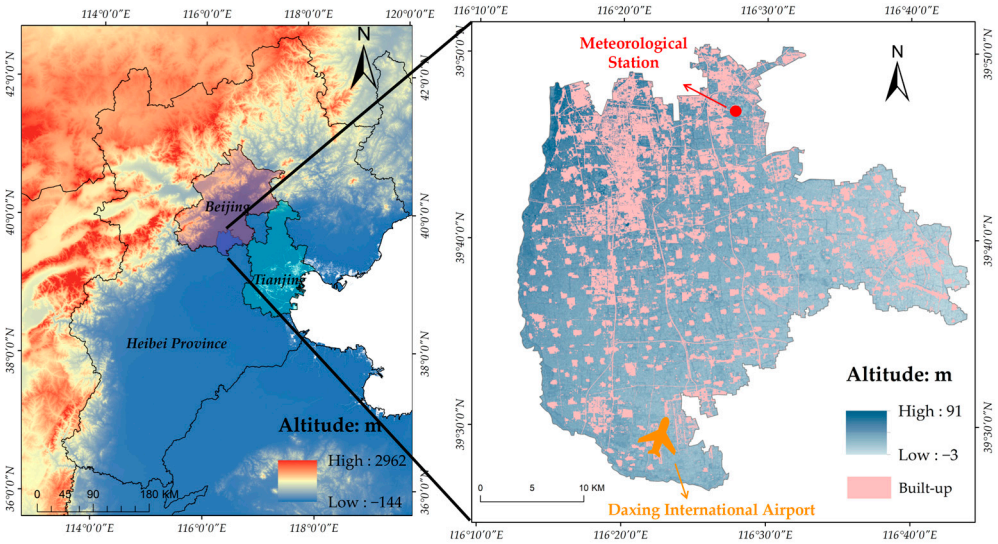

Figure 1. Geographical location map of Daxing District, with respective altitude (m).

Considering the key parameters for the above wind erosion equation, the data required are bare soil area, soil texture, wind speed, precipitation, and vegetation cover factor. Their corresponding sources are as follows:

To obtain the high-accuracy bare soil data, we used the data acquired by BJ-2 and BJ-3 of Disaster Monitoring Constellation (DMC) with resolutions of 0.8 m and 0.5 m, respectively, for each month of 2020 to 2022 (http://114.116.226.59/chinese/home/, accessed on 10 November 2024).

Soil texture data are available from the Harmonized World Soil Database (HWSD) (https://www.fao.org/soils-portal/en/, accessed on 10 November 2024).

The temperature and precipitation data were provided by the Daxing District Meteorological Bureau, Beijing, and the wind speed data were obtained from the historical weather network of Daxing District (https://www.tianqi24.com/daxing/history.html, accessed on 10 November 2024).

The vegetation cover factor was derived from the surface reflectance data (https://developers.google.com/earth-engine/datasets/catalog/sentinel, accessed on 10 November 2024), with both near-infrared and red-edge bands of 10 m spatial resolution of Level-2A data of Sentinel-2.

2.2. Wind Erosion Equation

This study utilizes the wind erosion equation as a model to estimate soil dust emissions, with the specific formula detailed below:

$$W_{si} = E_{si} \times A_s \tag{1}$$

In the equation, W_{si} represents the total emissions of PM_i (particulate matter with an aerodynamic diameter between 0 and i μm, the same hereinafter) from bare SFD, in tons per year (t/a). E_{si} is the emission factor of PM_i from bare soil dust sources, in tons per square meter per year, $\mathrm{t}/\left(10^4\ \mathrm{m}^2 \times \mathrm{a}\right)$. A_s is the area of bare soil sources in square meters (m^2).

$$E_{si} = a \times D_i \times C \times (1-\eta) \times 10^{-4} \tag{2}$$

$$D_i = k_i \times I_{we} \times f \times L \times V \tag{3}$$

In the equation, D_i is the dust emission factor of PM_i. C is the climate factor, representing the influence of meteorological factors on bare SFD [31,32] (Li Beibei et al. made adjustments to the parameters in the soil wind erosion equation to localize it, so the modified climate factor is used for calculation [33]). η is the removal efficiency of dust by

pollution control technologies, in percentage (%). When multiple measures are implemented simultaneously, the highest control efficiency is taken. k_i indicates the percentage content of PM_i in bare soil dust, with recommended values of 1 for TSP, 0.30 for PM_{10}, and 0.05 for $PM_{2.5}$. I_{we} stands for the soil wind erosion index [34], f denotes the ground roughness factor (assumed to be 0.5 in this study [33], or 1 in coastal, island, lakeshore, and desert areas), and L represents the unshielded width factor, set at 0.85 in this research [35]. V is the vegetation cover factor, indicating the proportion of exposed soil area to the total calculated area.

The climate factor C is an important indicator used to characterize the impact of meteorological factors on SFD emissions. It is primarily determined by wind speed, precipitation, evaporation, and temperature. Compared to annual climate factors, monthly climate factors better reflect short-term climatic conditions. Therefore, for calculating soil dust emissions, it is advisable to use monthly climate factors. The specific calculation formula is as follows:

$$C = 3.86 \times \frac{\mu^3}{PE^2} \tag{4}$$

$$PE = 3.16 \times \sum_{j=1}^{12} \left[\frac{P_j}{(1.8T_j + 22)} \right]^{\frac{10}{9}} \tag{5}$$

In the equation, μ indicates the monthly average wind speed (m/s). PE represents the Sáenz–Wittig precipitation–evaporation index. P_j denotes the monthly precipitation amount in millimeters (mm), assumed to be 12.7 mm or less. T_j stands for the monthly average temperature in degrees Celsius (°C), assumed to be −1.7 °C or less [36,37].

The technical process employed in this study is outlined as follows: Firstly, the satellite data from BJ-2, BJ-3, and Sentinel-2 were preprocessed through temporal filtering, image clipping, and cloud cover removal. Next, the processed BJ-2 and BJ-3 images were visually interpreted to extract monthly bare soil patches, with the authenticity of the data verified through field surveys. For the processed Sentinel-2 images, the vegetation cover factor was calculated monthly using the dimidiate pixel model (DPM). Subsequently, the calculated bare soil area, vegetation cover factor, soil texture type data, meteorological data, and empirical data were integrated into the wind erosion equation to estimate the monthly emissions of fugitive dust from bare soil. Finally, a grid with a resolution of 10 m was constructed to analyze the emissions of fugitive soil dust.

The specific process for establishing an SFD emission inventory is shown in Figure 2.

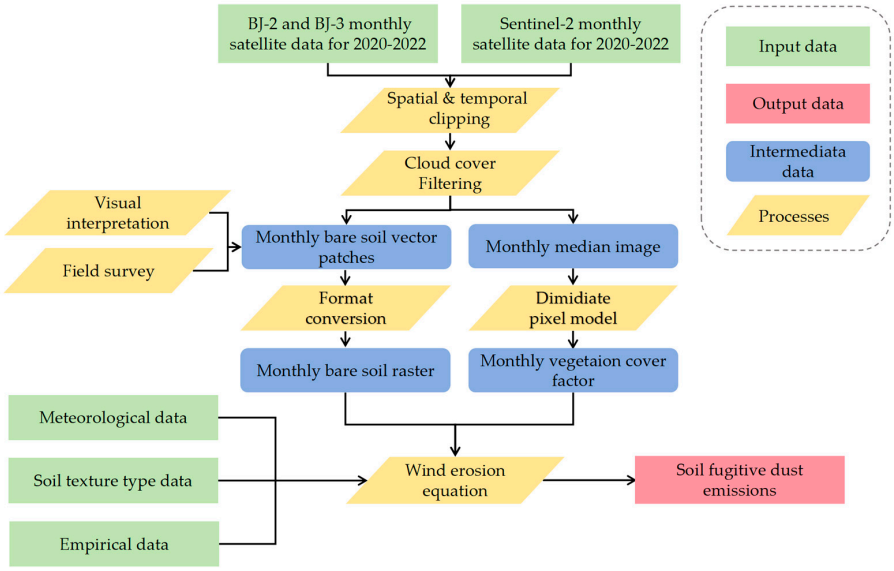

Figure 2. Technical process for establishing an SFD emission inventory.

2.3. Estimation of Bare Soil Patch

The bare soil patches in Daxing District were identified through visual interpretation of high-resolution remote sensing imagery from Beijing-2 (0.8 m spatial resolution) and Beijing-3 (0.5 m spatial resolution), supplemented by field validation. First, the high-resolution remote sensing images were preprocessed, including fusion, clipping, and stitching, to create a monthly high-definition base map of Daxing District. Visual interpretation was then conducted based on this base map to accurately delineate the locations of the bare soil patches. The identifiable bare soil mainly consisted of fallow farmland and undeveloped wasteland, which are areas with no surface cover. Additionally, field surveys were conducted every month to ensure the accuracy of the bare soil patches. As a result, a set of 36 monthly vector-based bare soil patches for the years 2020–2022 was obtained.

For seasonal analysis, the bare soil areas for spring, summer, autumn, and winter are defined by the sum of the bare soil areas in March, April, and May; June, July, and August; September, October, and November; and December, January, and February, respectively. To facilitate subsequent calculations, the bare soil patches were converted from vector format to a 10 m-resolution raster format.

2.4. Estimation of Vegetation Cover Factor

The vegetation coverage factor (V) is one of the key parameters in the WEQ model, representing the proportion of bare soil area per unit area. A higher value of the vegetation coverage factor (V) indicates less vegetation cover and more exposed land. It is important to note that (V) is closely related to vegetation coverage, but their meanings are entirely opposite. Vegetation coverage (VC) is defined as the percentage of the area occupied by vegetation (including leaves, stems, and branches) within a unit area [38], calculated using a pixel-based binary model [39,40].

$$VC = \frac{(NDVI - NDVI_{soil})}{(NDVI_{veg} - NDVI_{soil})} \tag{6}$$

$$V = 1 - VC \tag{7}$$

In the equation, (V) represents the coverage factor of a pixel, (VC) denotes the vegetation coverage of the pixel, $NDVI$ (Normalized Difference Vegetation Index) is the $NDVI$ value of that pixel, $NDVI_{veg}$ corresponds to the value of the vegetation-covered part in the image, and $NDVI_{soil}$ corresponds to the $NDVI$ value of the bare soil part in the image [41]. Here, we use the $NDVI$ histogram to determine confidence intervals, selecting $NDVI$ values at the 5th and 95th percentiles as the values for $NDVI_{soil}$ and $NDVI_{veg}$ [33].

This study adopts the method proposed by Li et al. [28] to calculate vegetation coverage, using band 4 (infrared) and band 8 (near infrared) from Sentinel-2 Level-2A satellite data to compute vegetation coverage information. Sentinel-2 satellites revisit every 5 days, providing multiple images per month. We calculated the median composite of the images obtained each month to mitigate extreme values (e.g., cloud cover) affecting vegetation coverage factor calculations. Subsequently, the median composite images, already atmospherically corrected, are clipped and used to compute the Normalized Difference Vegetation Index ($NDVI$) using the following formula:

$$NDVI = (NIR - R)(NIR + R) \tag{8}$$

In the equation, (NIR) represents the near-infrared band (band 4 in Sentinel-2), and (R) represents the red band (band 8 in Sentinel-2). This method calculates $NDVI$ using reflectance values from two bands, widely used for vegetation monitoring, with values ranging from -1 to 1. Positive values indicate vegetation cover and vary proportionally with vegetation density; a value of 0 represents rocks or bare soil; and negative values indicate highly reflective objects like clouds, water, or snow [42].

Through the above calculations, we obtained the monthly vegetation coverage factor for Daxing District with a spatial resolution of 10 m.

2.5. Soil Types

The soil type data were sourced from the Harmonized World Soil Database, with a spatial resolution of 1 km in raster format. Using the administrative boundary of Daxing District as a mask, the soil type distribution for the district was extracted. For convenience in subsequent calculations, the data were then resampled to a spatial resolution of 10 m. Soils of different textures have different soil wind erosion index values, which are detailed in Table 1 [33].

Table 1. Reference value of soil wind erosion index in study area ($t/10^4$ m^2a).

Soil Type	TSP	PM_{10}	$PM_{2.5}$
Loam	911	273	46
Loamy sand	331	99	17
Sandy loam	447	134	22
Sandy clay	138	41	7

2.6. Grid-Based Estimation of Soil Dust Emissions

Firstly, we overlay the resampled bare soil patches with the soil type data to assign a specific soil wind erosion index value to each bare soil pixel. Then, we utilized meteorological data from the Daxing District meteorological station to represent the climatic conditions of the entire region. Finally, we constructed a 10 m × 10 m SFD emission grid, integrating raster data on soil types, bare soil area, and vegetation cover factors. Using the wind erosion equation, we calculated the monthly SFD emissions for 36 months from 2020 to 2022. Additionally, the calculation of quarterly SFD emissions follows the same method as the calculation of bare soil area, where the total dust emissions for each season are represented by the sum of the emissions for the months corresponding to that season.

3. Results

3.1. Values of Key Parameters

3.1.1. Bare Soil

Spatially, bare soil is distributed across the entire Daxing District, with the highest concentrations found in the northern, northwestern, and southern regions (as shown in Figure 3). Field surveys indicated that the northern and northwestern areas are predominantly undeveloped wasteland and farmland undergoing reclamation. The southern area, however, contains bare soil resulting from the construction of Daxing International Airport. These exposed areas remain largely idle for most of the year and are highly susceptible to wind erosion, making them prone to dust emissions.

Temporally, the overall bare soil area in Daxing District has shown a decreasing trend (as shown in Figure 4), with clear seasonal variations. Bare soil areas are larger in the spring and winter seasons compared to the summer and autumn seasons (as shown in Figure 5). This is linked to the seasonal cycle of crop planting and harvesting, as well as the seasonal growth of vegetation on bare soil. Additionally, we observed a sharp reduction in the bare soil area from 2020 to 2021, mainly due to the reclamation efforts in the northern and northwestern regions. The Daxing District government implemented effective measures, such as afforestation, surface hardening, and covering with tarps, to significantly reduce the extent of bare soil.

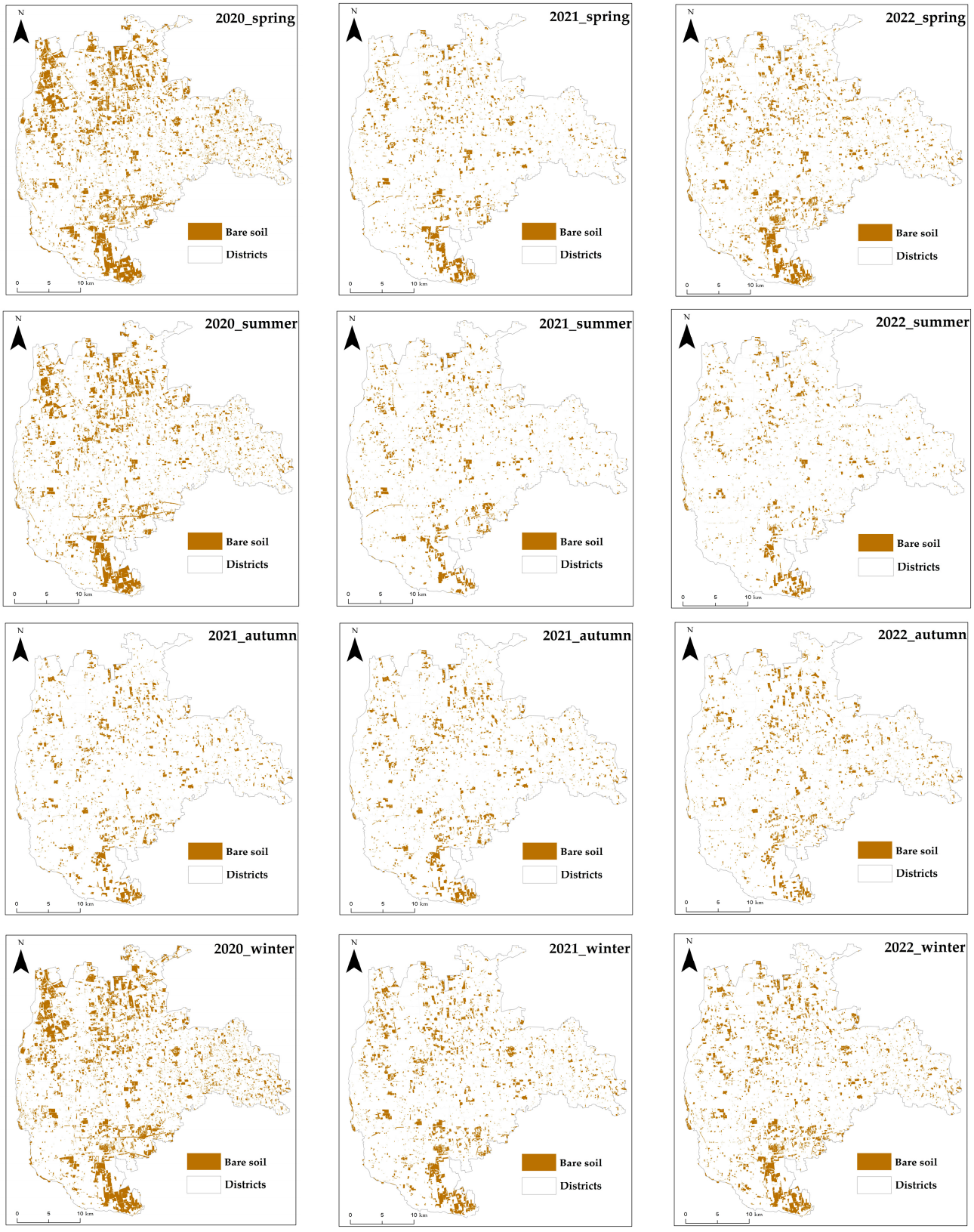

Figure 3. The quarterly bare soil distribution maps for Daxing District from 2020 to 2022.

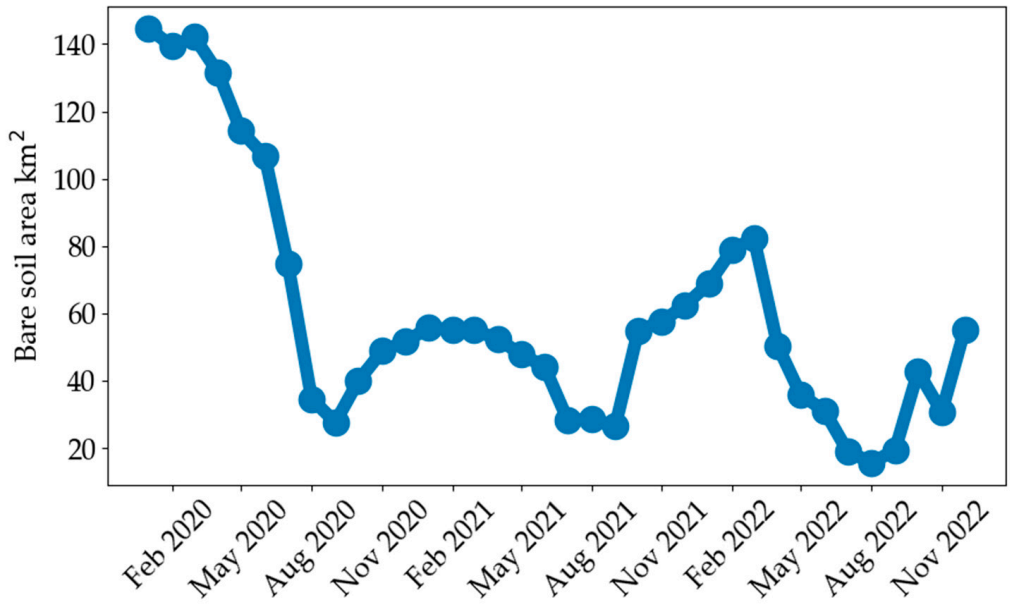

Figure 4. The monthly variation in bare soil area for Daxing District from 2020 to 2022.

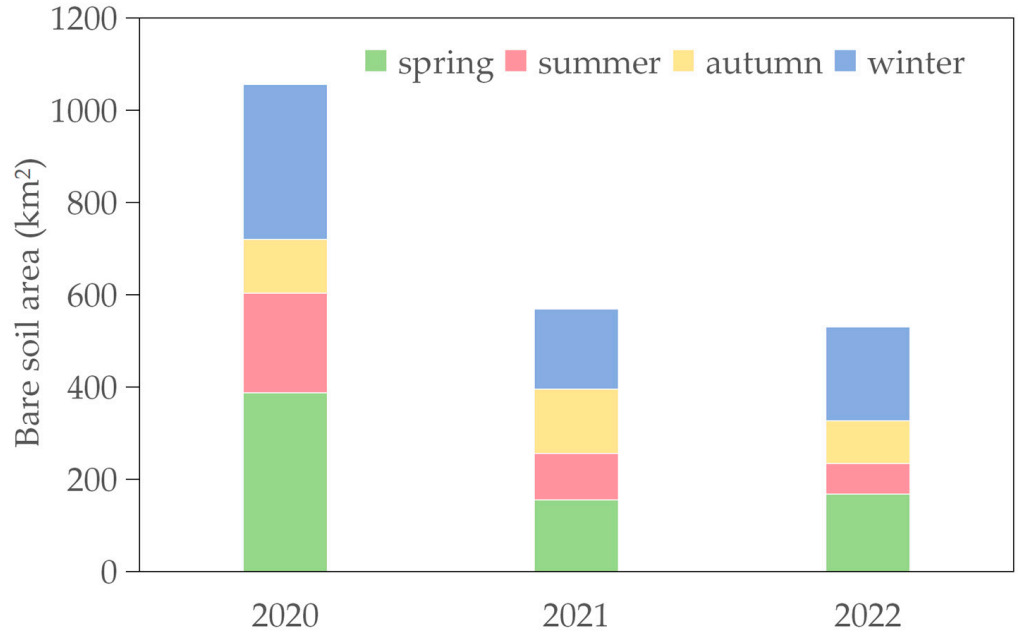

Figure 5. The quarterly bare soil area proportion maps for Daxing District from 2020 to 2022.

3.1.2. Vegetation Cover Factor

We utilized the pixel dichotomy method to estimate the monthly vegetation coverage factors in Daxing District, Beijing, from 2020 to 2022. The vegetation cover factor ranges from 0 to 1, where higher values indicate lower vegetation coverage and lower values indicate higher vegetation coverage. Taking 2021 as an example, monthly changes in vegetation coverage in Daxing District are illustrated in Figure 6. It is evident that vegetation coverage in July, August, and September is higher than the other months of the same year (shown by a larger proportion of green areas in the figure). Figure 7 further confirms that, during 2020 and 2022, the vegetation cover factor in July, August, and September was notably lower than that in the other months of the same year, indicating higher vegetation coverage.

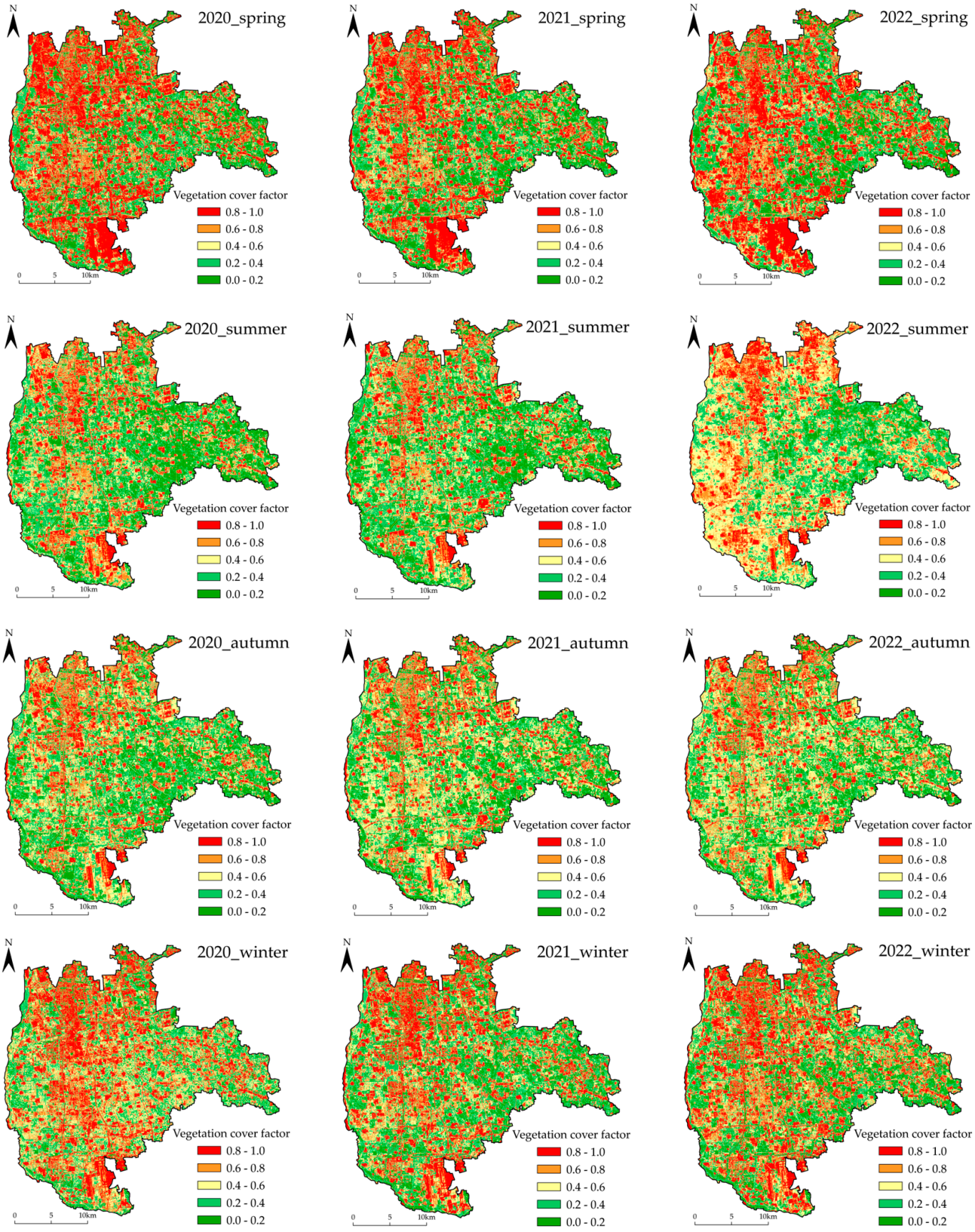

Figure 6. Quarterly vegetation cover factors in Daxing District from 2020 to 2022.

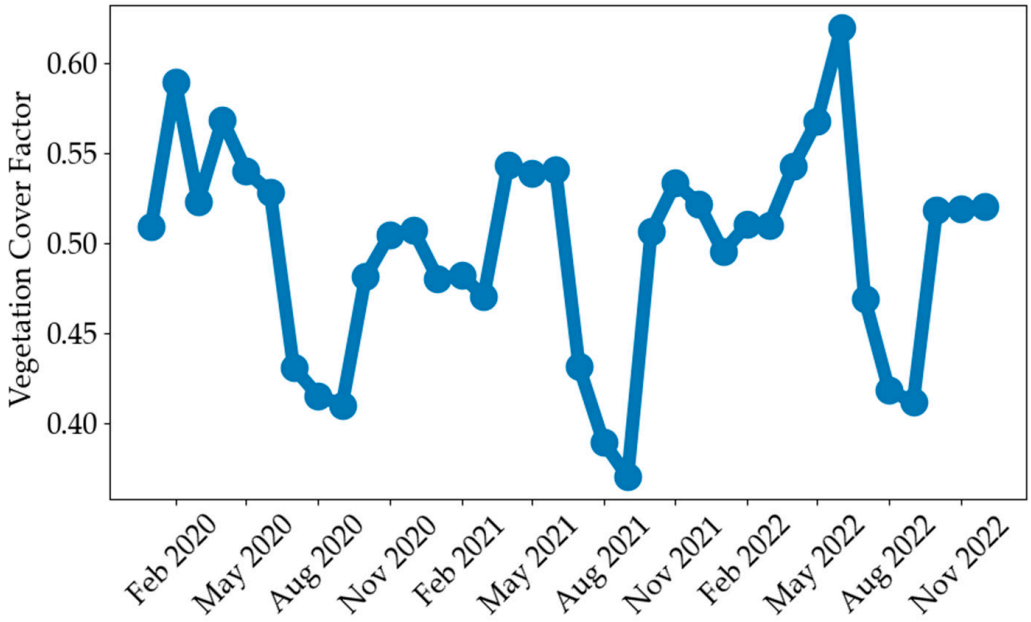

Figure 7. Monthly vegetation cover factor line chart for Daxing District from 2020 to 2022.

Figure 8 shows that the vegetation cover factors in spring and winter are higher than those of summer and autumn, which implies lower vegetation coverage rates in spring and winter than those of summer and autumn of the same year.

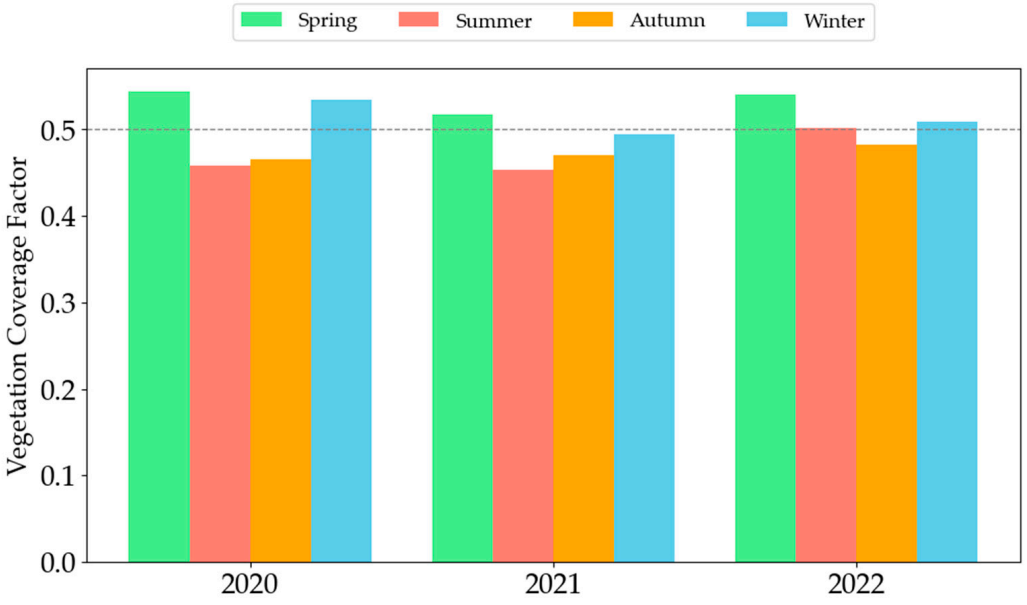

Figure 8. Quarterly average vegetation cover factor in Daxing District from 2020 to 2022.

3.1.3. Soil Types in Daxing District

The distribution of soil types in Daxing District, Beijing, is as in Figure 9: predominantly loam (80.3%), loam sand (18.79%), sandy loam with sand (0.59%), and sandy clay (0.31%). The soil erosion index (I_{we}) values vary for different soil types, with loam, the most prevalent type, having the highest soil erosion index.

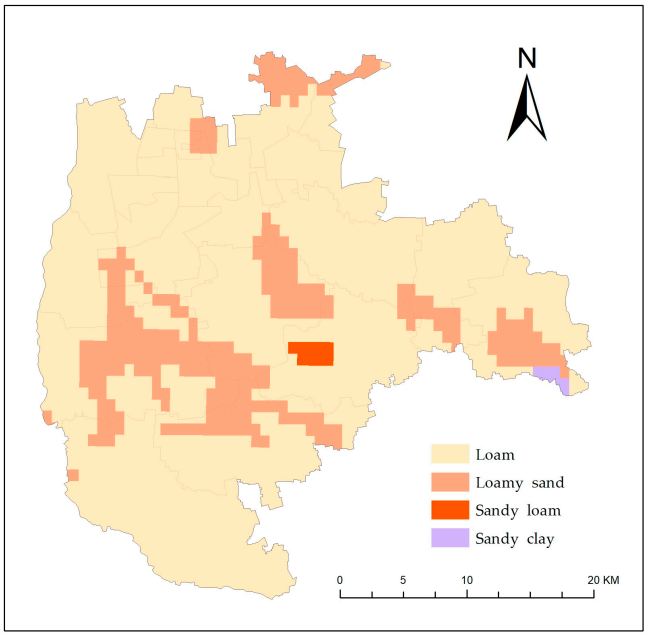

Figure 9. Spatial distribution of soil types in Daxing District.

3.1.4. Meteorological Data

The monthly meteorological data for the study area from 2020 to 2022 are shown in Figure 10, which shows the distinct seasonal characteristics of temperature and precipitation, with temperature rise and rainfall increase in summer and temperature drop and rainfall decrease in winter. The wind speed did not show strong seasonality, but it was generally higher in the spring of 2020 and 2021 and the winter of 2022 than those of the other seasons of the same years. The dry condition and strong wind during winter and spring contributed to the favorable condition for soil wind erosion.

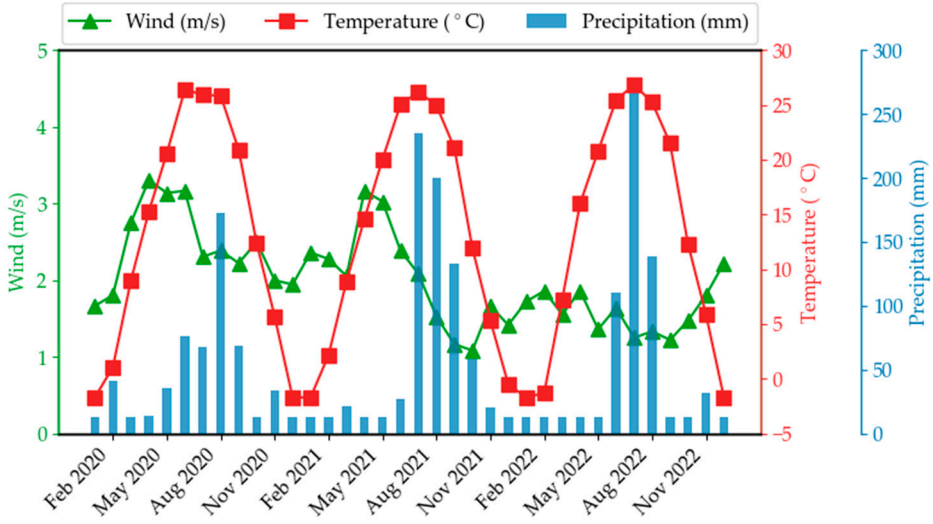

Figure 10. Monthly average temperature, wind speed, and monthly precipitation in Daxing District from 2020 to 2022.

3.2. Soil Dust Emissions

The monthly TSP, PM_{10}, and $PM_{2.5}$ emissions in Daxing District from 2020 to 2022 are presented in Table 2. The emissions of TSP, PM_{10}, and $PM_{2.5}$ exhibit a proportional relationship. Additionally, the Kruskal–Wallis test results indicate that there is no significant difference among the three groups at the 5% significance level ($H = 0.015$, $P = 0.99 > 0.05$) [43].

For the purpose of detailed analysis and discussion, this study takes PM_{10} as a representative example.

Table 2. Monthly Emissions of TSP, PM_{10}, and $PM_{2.5}$ for 2020 to 2022 in Daxing District.

Month–Year	Emissions of TSP (t)	Emissions of PM_{10} (t)	Emissions of $PM_{2.5}$ (t)
Jan 2020	72.94	6.56	0.46
Feb 2020	91.42	8.22	0.58
Mar 2020	371.08	33.36	2.34
Apr 2020	723.77	65.06	4.57
May 2020	534.60	48.06	3.38
Jun 2020	509.03	45.76	3.22
Jul 2020	124.23	11.17	0.78
Aug 2020	61.98	5.57	0.39
Sep 2020	42.03	3.78	0.27
Oct 2020	94.28	8.48	0.60
Nov 2020	56.59	5.09	0.36
Dec 2020	51.53	4.63	0.33
Jan 2021	88.31	7.94	0.56
Feb 2021	81.07	7.29	0.51
Mar 2021	54.86	4.93	0.35
Apr 2021	240.27	21.60	1.52
May 2021	209.98	18.88	1.33
Jun 2021	92.19	8.29	0.58
Jul 2021	33.79	3.04	0.21
Aug 2021	13.65	1.23	0.09
Sep 2021	5.11	0.46	0.03
Oct 2021	10.04	0.90	0.06
Nov 2021	37.57	3.38	0.24
Dec 2021	23.04	2.07	0.15
Jan 2022	43.39	3.90	0.27
Feb 2022	65.10	5.85	0.41
Mar 2022	36.75	3.30	0.23
Apr 2022	50.70	4.56	0.32
May 2022	15.28	1.37	0.10
Jun 2022	19.19	1.73	0.12
Jul 2022	5.56	0.50	0.04
Aug 2022	5.66	0.51	0.04
Sep 2022	5.15	0.46	0.03
Oct 2022	20.24	1.82	0.13
Nov 2022	25.64	2.30	0.16
Dec 2022	80.54	7.24	0.51

The spatial distribution of PM_{10} emissions is dependent on the distribution of bare soil patches, with concentrations primarily in the northern, northwestern, and southern parts of Daxing District (as shown in Figure 11). Overall, PM_{10} emissions show a decreasing trend (as shown in Figure 12), which is mainly related to the reduction in bare soil area. At the same time, emissions exhibit strong seasonality, with spring and winter emissions significantly higher than those in summer and autumn (as shown in Figure 13). This is partly due to seasonal variations in bare soil and partly due to the dry, windy meteorological conditions in spring and winter. In 2020, the PM_{10} emissions in winter were lower than in summer because the average wind speed in winter was lower than the average wind speed in summer. As a result, wind speed became the dominant factor in the calculation of emissions. This conclusion is explained in Section 3.3.

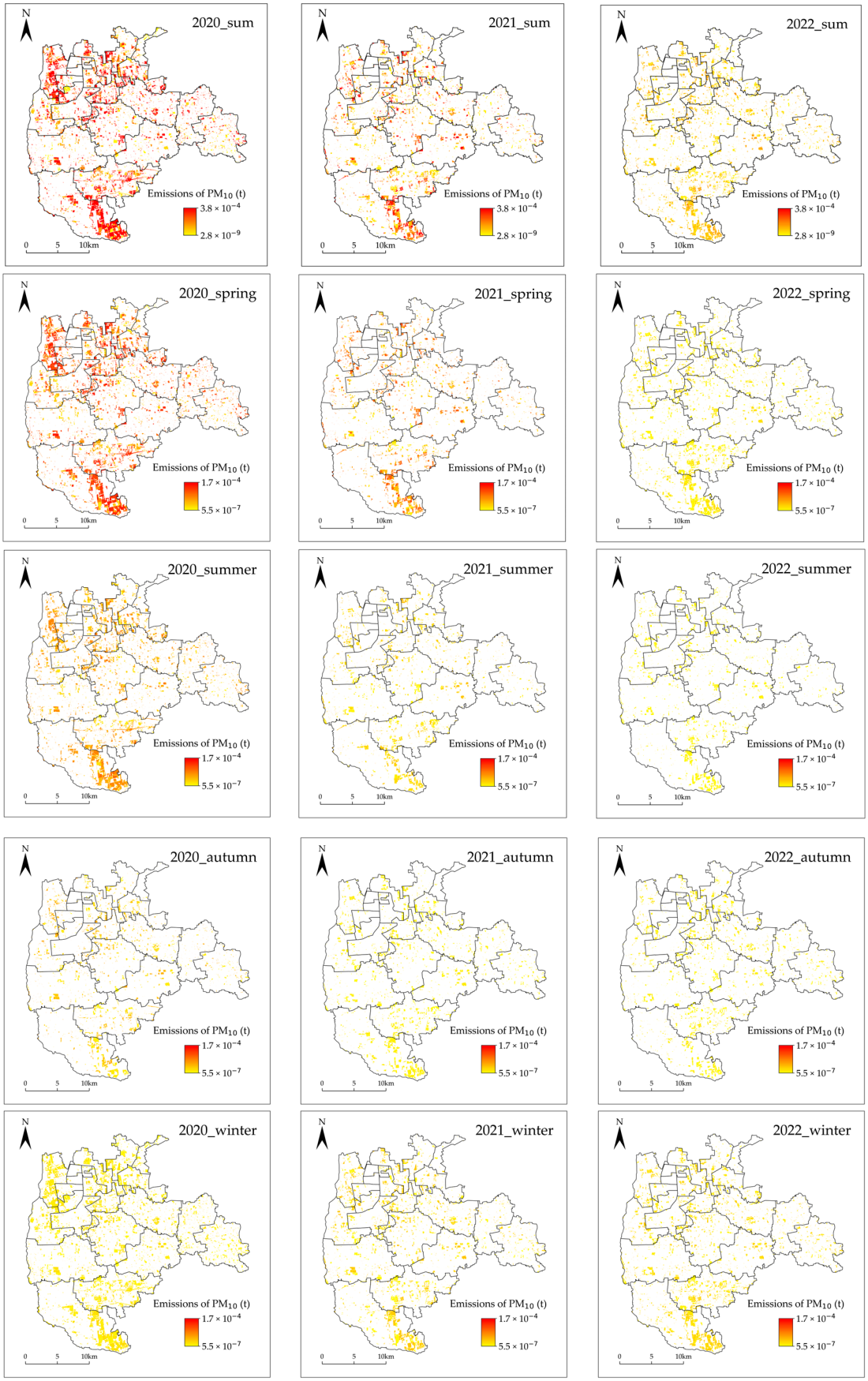

Figure 11. Annual and quarterly emission distribution maps for Daxing District from 2020 to 2022.

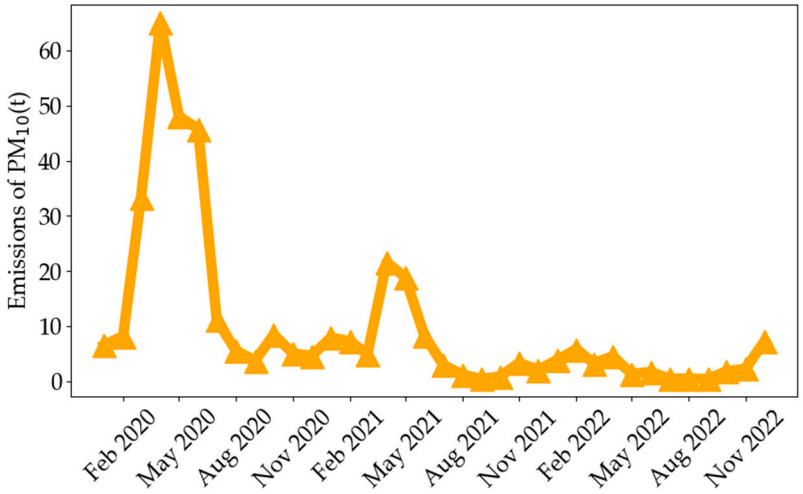

Figure 12. Monthly PM_{10} emission curve for Daxing District.

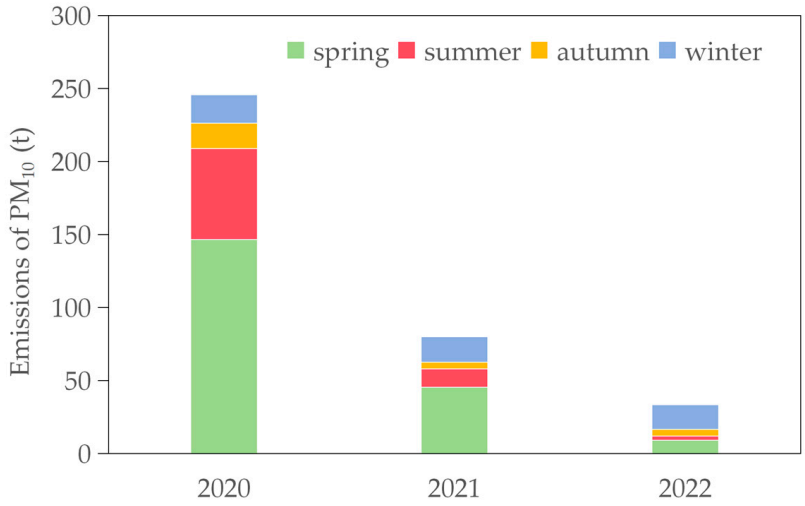

Figure 13. Annual and quarterly emission stacked bar charts maps for Daxing District from 2020 to 2022.

Additionally, the SFD emission sources are not solely limited to bare soil with constant soil properties. Some undeveloped wastelands (left idle for extended periods) are initially SFD sources, but once construction begins, they become construction dust sources. Although this study focuses on soil exposed to the air and affected by wind erosion, this shift in land use could inevitably lead to an overestimation of the SFD emissions.

To assess the reliability of the estimated bare soil dust emissions, the results were compared with those of studies from other cities. The comparison revealed no orders of magnitude difference among the dust emissions from different urban areas, validating the credibility of the calculated bare soil dust emissions in this study [12,21,28,35,44].

3.3. Correlation Analysis

Taking PM_{10} as an example (with TSP and $PM_{2.5}$ being proportional to PM_{10}), this study investigates the correlation between soil dust emissions and bare soil area, vegetation coverage factor, monthly average wind speed, monthly average temperature, and monthly precipitation. From Figure 14, it can be concluded that PM_{10} emissions exhibit a significantly strong correlation with monthly average wind speed (r = 0.81) and bare soil area (r = 0.65). Additionally, at a 95% confidence level, the confidence interval for PM_{10} emissions in relation to monthly average wind speed is 0.65–0.90, while the confidence interval in relation to bare soil area is 0.40–0.80. Furthermore, the *t*-test results show *p*-values of

less than 0.05 for both the monthly average wind speed and the bare soil area, confirming the statistical significance of these correlations [45–47]. Thus, increases in monthly average wind speed and bare soil area are significantly associated with higher PM_{10} emissions. Additionally, we found that when different months have similar bare soil areas, even slight differences in wind speed can lead to significant variations in emission levels. The impact of wind speed on PM_{10} emissions is greater than that of bare soil area. Based on this correlation analysis, it is recommended to adopt a dual strategy for soil dust pollution control: reducing bare soil area and mitigating wind erosion. Enhancing vegetation and implementing land stabilization measures can effectively reduce bare soil exposure. Additionally, applying cover materials and constructing windbreaks can significantly limit wind-induced soil erosion.

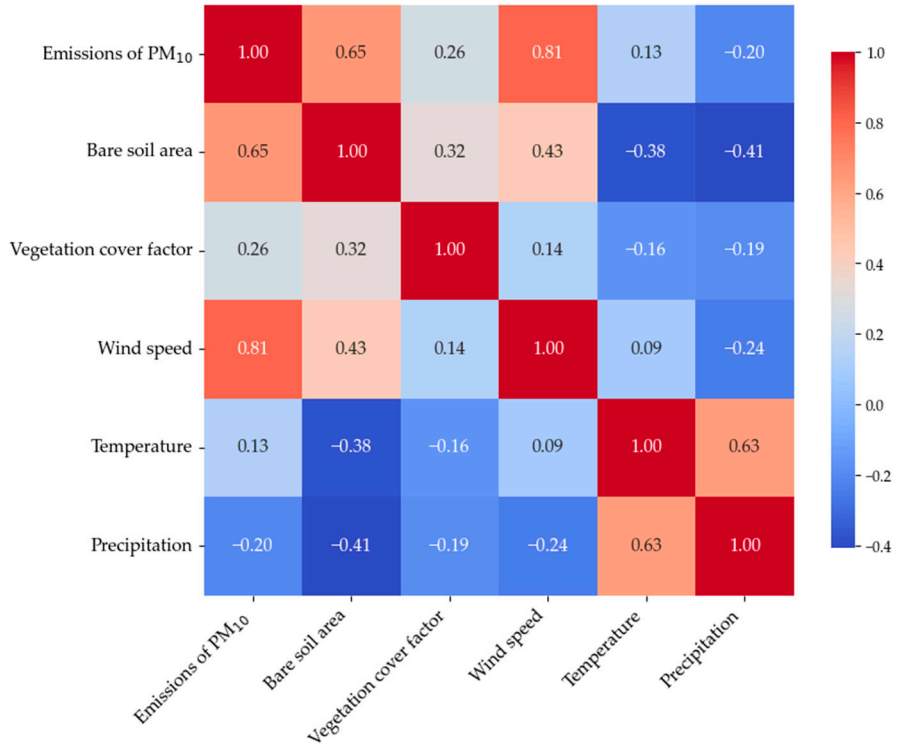

Figure 14. Heatmap of the correlation between emissions of PM_{10} and other factors.

3.4. Uncertainty Analysis

In the process of estimating SFD emissions for the study area, excluding the methods themselves, uncertainties arise primarily from the estimation of WEQ parameters, which stem mainly from empirical values and data accuracy.

- Uncertainty from Empirical Values:

The determination of values such as the unshielded width factor (L), the ground roughness factor (f), and the removal efficiency of dust by pollution control technologies (η) relies on recommended empirical values, introducing uncertainty and potential errors into the calculations. Additionally, the soil wind erosion index (I_{we}) is dependent on soil type; however, even within the same soil type, there are still differences in soil particle composition between urban and agricultural areas over time [48].

- Uncertainty from Data Accuracy:

The spatial resolution of soil type data and meteorological data is insufficient, affecting the precision of SFD emissions and introducing uncertainty into the results. While meteorological stations provide good environmental representativeness, the temporal resolution of meteorological data can also impact its accuracy, especially during extreme weather

events. Additionally, the bare soil data from the "Daxing District Bare Soil Dynamic Remote Sensing Monitoring Project" are used for estimating bare soil areas. However, bare soil due to permanent basic farmland may not be fully accounted for, and seasonal variations affect the identification of bare soil, which may lead to an underestimation of the emissions. At the same time, a small portion of construction dust sources was included in the soil dust sources, which could lead to an overestimation of the emissions. The interaction of these factors increases the uncertainty in the soil dust emission calculations.

4. Conclusions

This study proposed a method for compiling SFD inventories with high spatiotemporal resolution. Unlike other research studies, high-spatial-resolution remote sensing imagery was employed to extract bare soil and calculate vegetation coverage factors in this study, and estimates of SFD emissions were computed on the scale of individual pixels (10 m $\times$ 10 m) monthly. The integration of high temporal and spatial resolution can more accurately reveal the characteristics of SFD emissions in the study area.

The results indicate that from 2020 to 2022, the bare soil area in Daxing District generally decreased, with clear seasonal variation, as the bare soil area in spring and winter is larger than that in summer and autumn. The overall reduction in bare soil area indicates that the Daxing District government has achieved notable success in managing bare soil, while the seasonal variation in bare soil is linked to crop planting and harvesting cycles, as well as the seasonal growth of vegetation on bare soil. The vegetation coverage factor in Daxing District was higher in the spring and winter seasons, implying a lower degree of vegetation cover. Coupled with the dry and windy climatic conditions during these seasons, as well as the extensive presence of loam soil, these factors collectively create favorable conditions for soil wind erosion. The total TSP, PM_{10}, and $PM_{2.5}$ emissions in Daxing District for 2020 to 2022 were 3996.54 tons, 359.26 tons, and 25.25 tons, respectively. Taking PM_{10} as an example, the SFD emissions in Daxing District for 2020, 2021, and 2022 were 245.72 tons, 79.99 tons, and 33.55 tons, respectively, showing a decreasing trend year by year and exhibiting seasonal variations that closely align with changes in bare soil areas. The emissions are primarily concentrated in the northwest, north, and south regions, which may be influenced by economic activities and policies in Daxing District.

Correlation analysis reveals a significant and strong positive relationship between PM_{10} emissions, bare soil area, and monthly average wind speed. As the extent of bare soil and the monthly average wind speed increase, PM_{10} emissions also tend to increase, with wind speed exerting a greater influence on PM_{10} emissions than bare soil area. Based on correlation analysis, it is recommended to implement management measures focusing on reducing bare soil areas and preventing wind erosion of soil.

Estimating PM emission inventories, their spatiotemporal distribution, and the correlation of influencing factors is of great significance in air pollution control. The combination of high-temporal-and-spatial-resolution remote sensing data with GISs can provide reliable PM emission inventories for urban areas. In subsequent research, we plan to incorporate construction dust sources, road dust sources, and stockpile dust sources into our analysis to compile a comprehensive emission inventory. However, on a large scale, a major challenge in applying this method is the difficulty in obtaining high-precision spatiotemporal data, particularly accurate distribution data for bare soil areas.

Author Contributions: Conceptualization, Q.L.; Data curation, S.L., D.W., L.Y. (Linjun Yu), L.Y. (Ling Yi) and G.C.; Investigation, Q.L., Y.L., S.L. and D.W.; Methodology, Q.L.; Project administration, J.Z., B.Z., F.Z., D.Z. and D.W.; Software, L.Y. (Linjun Yu); Visualization, Q.L.; Writing—original draft, Q.L.; Writing—review and editing, Q.L., Y.L. and S.L. All authors have read and agreed to the published version of the manuscript.

Funding: This work was supported by the National Key R&D Program of China (No. 2022YFF0606402), the National Natural Science Foundation of China (No. 41471430), and the Fujian Provincial Science and Technology Plan Project (No. 2021T3065).

Data Availability Statement: The data developed in this study will be made available upon request to the corresponding author. The data are not publicly available due to privacy.

Acknowledgments: Special thanks to Lianwei Li and Shenshen Li, two kind and patient mentors, whose support greatly contributed to the completion of this manuscript.

Conflicts of Interest: The authors declare no conflicts of interest.

References

1. Joshua, S.A.; Marshall, J.D.; Cohen, A.J.; Brauer, M. Addressing Global Mortality from Ambient PM2.5. *Environ. Sci. Technol.* **2015**, *49*, 8057–8066. [CrossRef]
2. Liu, J.; Han, Y.; Tang, X.; Zhu, J.; Zhu, T. Estimating Adult Mortality Attributable to PM2.5 Exposure in China with Assimilated PM2.5 Concentrations Based on a Ground Monitoring Network. *Sci. Total Environ.* **2016**, *568*, 1253–1262. [CrossRef] [PubMed]
3. Hassan, H.; Kumar, P.; Kakosimos, K.E. The Impact of Local Fugitive Particulate Matter and Emission Inventories on Air Quality and Health in Dry and Arid Areas. *Sci. Total Environ.* **2022**, *824*, 153799. [CrossRef] [PubMed]
4. Chen, S.; Zhang, X.; Lin, J.; Huang, J.; Zhao, D.; Yuan, T.; Huang, K.; Luo, Y.; Jia, Z.; Zang, Z.; et al. Fugitive Road Dust PM2.5 Emissions and Their Potential Health Impacts. *Environ. Sci. Technol.* **2019**, *53*, 8455–8465. [CrossRef] [PubMed]
5. Carvacho, O.; Ashbaugh, L.; Flocchini, R. Elemental Composition of PM 10 and PM 2.5 in Ambient Air Downwind of Agricultural Operations in California's San Joaquin Valley. *WIT Trans. Ecol. Environ.* **2006**, *99*, 708. [CrossRef]
6. Chen, L.; Zhao, H.; Han, B.; Bai, Z. Combined Use of WEPS and Models-3/CMAQ for Simulating Wind Erosion Source Emission and Its Environmental Impact. *Sci. Total Environ.* **2014**, *466–467*, 762–769. [CrossRef]
7. Liu, B.; Wu, J.; Zhang, J.; Wang, L.; Yang, J.; Liang, D.; Dai, Q.; Bi, X.; Feng, Y.; Zhang, Y.; et al. Characterization and Source Apportionment of PM2.5 Based on Error Estimation from EPA PMF 5.0 Model at a Medium City in China. *Environ. Pollut.* **2017**, *222*, 10–22. [CrossRef]
8. Liu, A.; Wu, Q.; Cheng, X. Using the Google Earth Engine to Estimate a 10 m Resolution Monthly Inventory of Soil Fugitive Dust Emissions in Beijing, China. *Sci. Total Environ.* **2020**, *735*, 139174. [CrossRef]
9. Sun, L. Study on Emission Inventory of PM2.5 Pollution Sources in Atmospheric Environment—A Case Study of Jilin City. Master's Thesis, Jilin University, Changchun, China, 2016.
10. Li, L. A Highly Resolved Fugitive Dust Emissions Inventory In Harbin And Assessment of Contral Strategies. Master's Thesis, Harbin Institute of Technology, Harbin, China, 2018.
11. Huang, Y. Emission Inventory and Spatial Distribution Characteristics of Particulate Matters from Dust Source in Wuhan, China. *J. Wuhan Univ. Nat. Sci. Ed.* **2018**, *64*, 354–362. [CrossRef]
12. Zhang, J. Development of Refined Emission Inventory of Air Pollutants for Beichen District of Tianjin. *Environ. Monit. China* **2018**, *34*, 20–27. [CrossRef]
13. Shu, L. Emission Inventory and Characteristics of Atmosphere PM2. 5 and PM10 in Nanchong. *Environ. Monit. China* **2018**, *34*, 84–92. [CrossRef]
14. Woodruff, N.P.; Siddoway, F.H. A wind erosion equation. *Soil Sci. Soc. Am. J.* **1965**, *29*, 602–608. [CrossRef]
15. Skidmore, E.L.; Woodruff, N.P. *Wind Erosion Forces in the United States and Their Use in Predicting Soil Loss*; U.S. Agricultural Research Service: Washington, DC, USA, 1968.
16. Fryrear, D.W.; Bilbro, J.D.; Saleh, A.; Schomberg, H.; Stout, J.E.; Zobeck, T.M. RWEQ: Improved Wind Erosion Technology. *J. Soil Water Conserv.* **2000**, *55*, 183–189.
17. Buschiazzo, D.E.; Zobeck, T.M. Validation of WEQ, RWEQ and WEPS Wind Erosion for Different Arable Land Management Systems in the Argentinean Pampas. *Earth Surf. Process. Landf. J. Br. Geomorphol. Res. Group* **2008**, *33*, 1839–1850. [CrossRef]
18. Lu, H.; Shao, Y. Toward Quantitative Prediction of Dust Storms: An Integrated Wind Erosion Modelling System and Its Applications. *Environ. Model. Softw.* **2001**, *16*, 233–249. [CrossRef]
19. Song, H.; Zhang, K.; Piao, S.; Wan, S. Spatial and Temporal Variations of Spring Dust Emissions in Northern China over the Last 30 Years. *Atmos. Environ.* **2016**, *126*, 117–127. [CrossRef]
20. Li, T.; Bi, X.; Dai, Q.; Wu, J.; Zhang, Y.; Feng, Y. Optimized Approach for Developing Soil Fugitive Dust Emission Inventory in "2+26" Chinese Cities. *Environ. Pollut.* **2021**, *285*, 117521. [CrossRef]
21. Li, L. Emission inventory and temporal and spatial distribution of soil dust in Harbin. *Environ. Pollut. Control* **2021**, *43*, 679–683+724. [CrossRef]
22. Li, M. Estimation and spatial distribution characteristics of soil dust emissions in Shijiazhuang. *Chin. J. Environ. Eng.* **2017**, *11*, 5993–5999.
23. Lin, Y. Construction of emission inventory and temporal-spatial distribution of soil fugitive dust in Xining, China. *Environ. Chem.* **2022**, *41*, 4006–4015.
24. Qin, J. Study on Spatial and Temporal Characteristics of Construction Dust and Soil Dust Pollution Sources in Urban Areas of Changsha. *Environ. Monit. China* **2020**, *36*, 69–79. [CrossRef]
25. Xu, Y. Research on emission inventory of bareness wind erosion dust in Zhengzhou. *Environ. Pollut. Control* **2016**, *38*, 22–27. [CrossRef]

26. Zhou, Y.; Guo, B.; Wang, S.; Tao, H. An Estimation Method of Soil Wind Erosion in Inner Mongolia of China Based on Geographic Information System and Remote Sensing. *J. Arid Land* **2015**, *7*, 304–317. [CrossRef]
27. Mandakh, N.; Tsogtbaatar, J.; Dash, D.; Khudulmur, S. Spatial Assessment of Soil Wind Erosion Using WEQ Approach in Mongolia. *J. Geogr. Sci.* **2016**, *26*, 473–483. [CrossRef]
28. Li, T.; Bi, X.; Dai, Q.; Liu, B.; Han, Y.; You, H.; Wang, L.; Zhang, J.; Cheng, Y.; Zhang, Y.; et al. Improving Spatial Resolution of Soil Fugitive Dust Emission Inventory Using RS-GIS Technology: An Application Case in Tianjin, China. *Atmos. Environ.* **2018**, *191*, 46–54. [CrossRef]
29. Zhou, Y.; Zhang, G.; Jiang, L.; Chen, X.; Xie, T.; Wei, Y.; Xu, L.; Pan, Z.; An, P.; Lun, F. Mapping Local Climate Zones and Their Associated Heat Risk Issues in Beijing: Based on Open Data. *Sustain. Cities Soc.* **2021**, *74*, 103174. [CrossRef]
30. Yuanyuan, W. Regional Representativeness Analysis of National Reference Clim atological Stations Based on MODIS/LST Product. *J. Appl. Meteorol. Sci.* **2011**, *22*, 214–220.
31. Thornthwaite, C.W. The Climates of North America: According to a New Classification. *Geogr. Rev.* **1931**, *21*, 633–655. [CrossRef]
32. Skidmore, E.L. Wind Erosion Climatic Erosivity. *Clim. Chang.* **1986**, *9*, 195–208. [CrossRef]
33. Li, B. Localization of Soil Wind Erosion Dust Emission Factor in Beijing. *Environ. Sci.* **2020**, *41*, 2609–2616. [CrossRef]
34. Chepil, W.S. *Soil Conditions That Influence Wind Erosion*; U.S. Department of Agriculture: Washington, DC, USA, 1958.
35. Song, L. Construction and Dynamic Method of Soil Fugitive Dust Emission Inventory with High Spatial Resolution in Beijing-Tianjin-Hebei Region. *Res. Environ. Sci.* **2021**, *34*, 1771–1781. [CrossRef]
36. Lyles, L. Erosive Wind Energy Distributions and Climatic Factors for the West. *J. Soil Water Conserv.* **1983**, *38*, 106–109.
37. Panebianco, J.E.; Buschiazzo, D.E. Erosion Predictions with the Wind Erosion Equation (WEQ) Using Different Climatic Factors. *Land Degrad. Dev.* **2008**, *19*, 36–44. [CrossRef]
38. Gitelson, A.A.; Kaufman, Y.J.; Stark, R.; Rundquist, D. Novel Algorithms for Remote Estimation of Vegetation Fraction. *Remote Sens. Environ.* **2002**, *80*, 76–87. [CrossRef]
39. Xiong, C. Vegetation Coverage Based on Landsat8 Images in Guangzhou. *Environ. Sci. Technol.* **2015**, *38*, 383–386.
40. Kun, J.; Yunjun, Y.; Xiangqin, W.; Shuai, G.; Bo, J.; Xiang, Z. A Review on Fractional Vegetation Cover Estimation Using Remote Sensing. *Adv. Earth Sci.* **2013**, *28*, 774. [CrossRef]
41. Gan, C. Changes of Vegetation Coverage During Recent 18 Years in Lianjiang River Watershed. *Sci. Geogr. Sin.* **2011**, *31*, 1019–1024. [CrossRef]
42. Lambin, E.F. Indicators of Land-Cover Change for Change-Vector Analysis in Multitemporal Space at Coarse Spatial Scales. *Int. J. Remote Sens.* **1994**, *15*, 2099–2119. Available online: https://www.tandfonline.com/doi/abs/10.1080/01431169408954230 (accessed on 20 June 2024). [CrossRef]
43. Forthofer, R.N.; Lee, E.S.; Hernandez, M. 9—Nonparametric Tests. In *Biostatistics*, 2nd ed.; Forthofer, R.N., Lee, E.S., Hernandez, M., Eds.; Academic Press: San Diego, CA, USA, 2007; pp. 249–268. ISBN 978-0-12-369492-8.
44. Li, T.; Dong, W.; Dai, Q.; Feng, Y.; Bi, X.; Zhang, Y.; Wu, J. Application and Validation of the Fugitive Dust Source Emission Inventory Compilation Method in Xiong'an New Area, China. *Sci. Total Environ.* **2021**, *798*, 149114. [CrossRef]
45. Maltare, N.N.; Vahora, S.; Jani, K. Seasonal Analysis of Meteorological Parameters and Air Pollutant Concentrations in Kolkata: An Evaluation of Their Relationship. *J. Clean. Prod.* **2024**, *436*, 140514. [CrossRef]
46. Ye, P.C.; Chen, H.; Wu, J.Y.; Zhang, G.F. Distribution Pattern and Correlation With Main Environmental Factors of Higher Plant Diversity in Northwest Yunnan. *J. Ecol. Rural Environ.* **2020**, *36*, 89–94. [CrossRef]
47. Liu, Y.; Zhou, Y.; Lu, J. Exploring the Relationship between Air Pollution and Meteorological Conditions in China under Environmental Governance. *Sci. Rep.* **2020**, *10*, 14518. [CrossRef] [PubMed]
48. Trammell, T.L.E.; Pouyat, R.V.; D'Amico, V. Heterogeneity in Soil Chemistry Relates to Urbanization While Soil Homogeneity Relates to Plant Invasion in Small Temperate Deciduous Forests. *Landsc. Ecol.* **2022**, *37*, 1417–1429. [CrossRef]